RSC Advances

PAPER

View Article Online
View Journal | View Issue

Cite this: *RSC Adv.*, 2025, **15**, 49557

Fabrication of copper silicate microspheres using rice husk ash and its application for dearomatization of phenol derivatives

Na Li,[a] Lide Su,[a] Hongying Wang,[a] Hongdao Li,[b] Qianqian Shen*[c] and Xiaofeng Han*[a]

Received 27th November 2025
Accepted 4th December 2025

DOI: 10.1039/d5ra09185c

rsc.li/rsc-advances

In the present study, tubular copper silicate microspheres (CuSi-NTMs) were hydrothermally synthesized using high-silicon rice husk ash (RHA) as the raw material. Structural characterization reveals CuSi-NTMs have abundant mesopores, with a larger pore volume (0.367 cm^3 g^{-1}) and specific surface area (375 m^2 g^{-1}) than the precursor RHA, facilitating active component dispersion. As expected, CuSi-NTMs exhibited superior catalytic performance in the dearomatization reaction between phenol derivatives and azodicarboxylates compared to other copper-based catalysts, achieving a 98% yield. The steric hindrance and electronic effects of phenolic substituents were also investigated. An ionic catalytic mechanism for CuSi-NTMs has been proposed. Cu(II) coordinates with the phenolic hydroxyl group to activate its para-position. Then, the activated phenol undergoes a Michael addition with the N=N group and deprotonates, resulting in the formation of cyclohexadienone derivatives. Additionally, preparative scale synthesis of cyclohexadieneone has been demonstrated.

1 Introduction

As a major rice producer, China generates approximately 40 million tons of rice husks (RHs) each year. The haphazard accumulation of RHs without effective treatment leads to land occupation, especially causing various environmental problems, such as bacterial growth, soil compaction, water and air pollution, *etc.*[1–3] Effective utilization of RHs has emerged as a crucial concern in agricultural waste management.[4–9] At present, converting RHs into thermal and electrical energy is an important way to achieve their high-value utilization, whereas approximately 0.2 tons of rice husk ash (RHA) is produced per ton burned in this process.[2,10] Unfortunately, RHA is easily carried away by the wind due to their low bulk density, resulting in air pollution and ecological damage.[11,12] Currently, its resource utilization has been officially put on the agenda to eliminate environmental risk.

Actually, RHA is rich in silicon (>80%), along with minerals such as potassium, magnesium, and calcium.[13–15] As reported, extracting silicon from RHA is a key strategy for its valorization, producing high-value materials like silica and silica gel.[16–20] However, this process often requires complex chemical treatment to separate and purify silica, thereby consuming substantial amounts of energy and chemical reagents and leading to secondary pollution.[21,22] It is noteworthy that previous studies have primarily centered on purifying silicon from RHA, neglecting the potential value of silicon in catalyst applications.[23] By converting *in situ* silicon from RHA into catalytic components or carriers, we significantly simplify the process flow, reduce production costs, and minimize resource waste. Therefore, exploring the specific application routes and mechanisms of RHA-derived silicon in the catalyst field holds considerable potential value and broad prospects.

The dearomatization of phenol derivatives plays a significant role in organic synthesis.[24–26] It can transform phenol derivatives into non-aromatic structures with higher reactivity, providing a key step for the synthesis of complex organic molecules.[27,28] Dearomatization have extensive applications in fields such as drug synthesis, total synthesis of natural products, and preparation of functional materials.[29–31] There are numerous types of catalysts used in dearomatization, including small organic molecule catalysts and transition metal catalysts, *etc.*[31–34] Li's group reported an efficient silver-catalyzed aminative dearomatization of phenols with azodicarboxylates, using catalysts such as Ag_2CO_3, AgOAc, AgOTFA and Ag_2O. Among them, Ag_2O showed the best result (95% yield).[35] Sarkar's group developed a blue light-driven method using riboflavin tetraacetate (RFTA) as a photocatalyst for efficient para-selective aminative dearomatization of phenols/anilines.[36] In Wang's study, a series of copper catalysts (*e.g.*, CuOAc, $CuCl_2$ and CuI)

[a]*College of Chemistry and Materials Science, Inner Mongolia Minzu University, Tongliao 028000, P. R. China. E-mail: xfhan2018@imun.edu.cn*

[b]*Department of Chemistry and Chemical Engineering, Taiyuan Institute of Technology, Taiyuan 030008, P. R. China*

[c]*School of Environmental and Chemical Engineering, Xi'an Key Laboratory of Textile Chemical Engineering Auxiliaries, Xi'an Polytechnic University, Xi'an 710048, P. R. China. E-mail: 20241201@xpu.edu.cn*

were employed for phenol dearomatization, but all exhibited low efficiency (<50%), whereas $Cu(OTf)_2$ proved to be the most effective.[25] However, due to constraints on metal electronic structures, coordination environments, and substrate interaction patterns, efficient dearomatization catalysts are still limited.

Herein, we propose a novel approach for the *in situ* utilization of silicon from RHA for synthesize tubular copper silicate microspheres (CuSi-NTMs). Subsequently, we developed a dearomatization reaction between phenol derivatives and azodicarboxylates using CuSi-NTMs as the catalyst. The structure of catalyst, performance and catalytic mechanism were investigated in detail. This research provides a new idea for the high-value-added utilization of agricultural waste.

2 Experimental section

2.1 Materials

The raw rice husks (RHs) were supplied from Qiqihar Yuquan Rice Industry Co. Ltd (Heilongjiang, China). Ammonium hydroxide ($NH_3 \cdot H_2O$, 25–28%), hydrochloric acid (HCl) were purchased from Beijing Chemical Factory, Beijing, China. Phenol substrates were obtained from Bide Pharmatech Ltd, Shanghai, China. Azodicarboxylates, $CuCl_2$, CuBr, CuI, Cu_2O, $CuSO_4$ and $Cu(OAc)_2$ were purchased from Energy-chemical Co. Ltd, Anhui, China. Copper nitrate trihydrate [$Cu(NO_3)_2 \cdot 3H_2O$] was supplied by Titan Technology Co., Ltd, Shanghai, China. 2,2,6,6-Tetramethylpiperidinooxy (TEMPO) was supplied from Heowns Ltd, Tianjin, China. Organic reagents including acetone, dichloromethane (CH_2Cl_2), toluene, tetrahydrofuran (THF), methanol (CH_3OH) and *N*,*N*-dimethylformamide (DMF) were obtained from Tianjin Damao Chemical Reagen Co. Ltd, Tianjin, China.

2.2 Preparation of the catalyst

RHs (10 g) were first washed by deionized (DI) water several times to remove floatable substances. Subsequently, RHs were washed again with sodium dodecylbenzene sulfonate solution (3%, 200 mL), followed by additional rinsing with DI water three times. After filtration, the washed RHs were dried in an oven at 80 °C overnight. The dried RHs were then placed in a crucible and roasted at 160 °C for 1 h to obtain rice husk ash (RHA).

A certain amount of hydrochloric acid (5 mL, 6 mol L^{-1}) was added to the resulting RHA (0.5 g), followed by magnetic stirring at 70 °C for 1 h. The mixture was centrifuged, filtered, and then washed with DI water three times. Furthermore, the solid residue was transferred to a beaker, to which $Cu(NO_3)_2 \cdot 3H_2O$ (2.1 g), $NH_3 \cdot H_2O$ (4.5 mL), and 50 mL DI water were added. After stirring the mixture for 30 min, the suspension was transferred to a hydrothermal reactor (100 mL) and heated at 140 °C for 10 h. The resulting solid was repeatedly washed with DI water and absolute ethanol, then dried. Schematically, the schematic illustration for the synthesis of CuSi-NTMs is depicted in Fig. 1.

2.3 Catalytic test

Typically, phenol derivatives (0.1 mmol, 1.0 equiv.) was dissolved in acetone (1.0 mL). Subsequently, diethyl azodicarboxylate (0.2 mmol, 2.0 equiv.) and the catalyst (20 mmol%) were added to the solution. The mixture was then stirred for 2 h at 25 °C and monitored by thin-layer chromatography (TLC). After the reaction was complete, the organic solvent was dried with anhydrous Na_2SO_4, filtered, and concentrated under reduced pressure. Finally, the residue was purified with chromatography on silica gel (ethyl acetate: petroleum ether = 1 : 5–1 : 3).

2.4 Characterization

Proton nuclear magnetic resonance (^{1}H NMR) spectra was recorded on a Quantum-1 plus 400 MHz spectrometer (Zhongke-Niujin, China) at 25 °C. X-ray diffraction (XRD) analysis of the samples was performed using an X-ray powder diffractometer (SmartLab, Rigaku, Japan). The microstructure and morphology were characterized by a scanning electron microscope (SEM) (Sigma 360, ZEISS, Germany) and transmission electron microscopy (TEM) (F200X G2, FEI Talos, USA). X-ray photoelectron spectra (XPS) were collected by an X-ray photoelectron spectrometer (Kratos AXIS SUPRA+, Shimadzu, Japan). Fourier transform infrared (FTIR) spectra of the samples were obtained using the KBr pellet method on an IRAFFINITY-1S spectrometer (Shimadzu, Japan). The elemental analysis of the samples was conducted using an X-ray fluorescence spectrometer (XRF) (Axios, Panalytical, Netherlands).

3 Result and discussion

3.1 Characterizations of materials

As shown in the inset of Fig. 2, RHA obtained after calcination exhibits a grayish-white appearance, which is attributed to the

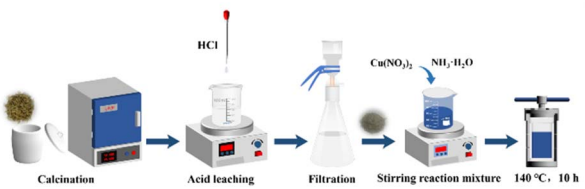

Fig. 1 Schematic illustration for the synthesis of CuSi-NTMs.

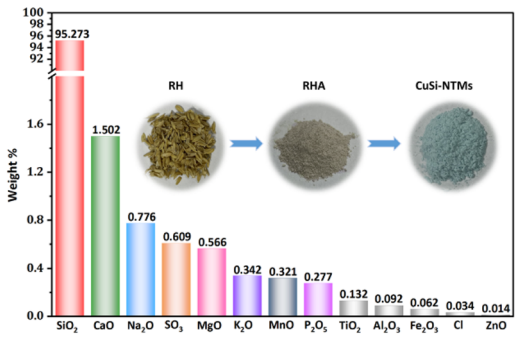

Fig. 2 XRF analysis of RHA.

removal of organic matter and partial decomposition of inorganic components in RHs at high temperatures (600 °C). The XRF analysis results (Fig. 2) indicate a 95.273 wt% silicon content in RHA, which is significantly higher than that in uncalcined RHs (18.2 wt%).[4] This demonstrates substantial silicon enrichment following high temperature calcination. The remaining constituents primarily consist of oxides such as CaO, Na_2O, and SO_3, along with trace elements such as Fe_2O_3, Al_2O_3, Cl and ZnO (<0.1 wt%), all present in relatively low concentrations. These minor components, which originate from the inherent minerals and impurities in RHs, are retained in the ash due to incomplete volatilization or decomposition during the calcination process. Overall, silica content predominates in the composition of RHA, offering a favorable material foundation for the design of silicon-based materials.

The crystal structures of the RHA and CuSi-NTMs sample were characterized by XRD. As shown in Fig. 3, the XRD pattern of RHA obtained by roasting at 600 °C exhibits a broad diffraction band between 20° and 30°, which is characteristic of amorphous materials. As reported, the crystalline phase of RHA is directly temperature-dependent, with an amorphous phase predominantly forming below 700 °C and a crystalline phase manifesting above this temperature.[37] The combined results of XRD and XRF (Fig. 2) demonstrate the formation of amorphous silica. As for the pattern of CuSi-NTMs, all the diffraction peaks can be clearly indexed to $CuSiO_3 \cdot 2H_2O$ (JCPDS card no. 03-0219), suggesting the copper silicate was obtained *in situ* using RHA. Particularly, the peaks of CuSi-NTMs are relatively broad because the amorphous RHA which is used as the silicon source fails to provide a regular lattice template, thereby inhibiting the crystalline growth of CuSi-NTMs. Low-crystallinity CuSi-NTMs with numerous surface defects and abundant active sites may exhibit higher catalytic activity.[38,39] The mechanism for CuSi-NTMs formation is proposed as follows. In an aqueous ammonia solution ($NH_3 \cdot H_2O$, pH ≈ 9), Cu^{2+} released from $Cu(NO_3)_2 \cdot 3H_2O$ coordinate with $NH_3 \cdot H_2O$ to form the stable copper-ammonia complex ion $[Cu(NH_3)_4]^{2+}$. Meanwhile, $NH_3 \cdot H_2O$ hydrolyzes to release hydroxide (OH^-), establishing an alkaline environment that promotes the etching of RHA. As RHA gradually dissolves under alkaline conditions, the silicon–oxygen bonds in its structure are broken, leading to the formation of soluble silicate ions (SiO_3^{2-}). Furthermore, negatively charged surfaces drive Cu^{2+} enrichment on RHA *via* electrostatic attraction of $[Cu(NH_3)_4]^{2+}$ complexes. Subsequently, to maintain charge neutrality in the solution, the SiO_3^{2-} in the solution combine with the surface adsorbed Cu^{2+}, leading to the nucleation of copper silicate *via* the reaction of $[Cu(NH_3)_4]^{2+} + SiO_3^{2-} + H_2O \rightarrow CuSiO_3 \cdot 2H_2O + NH_3 \cdot H_2O$.

Fourier-transform infrared (FTIR) spectroscopy was employed to investigate the surface functional groups of RHA and CuSi-NTMs, with the spectra shown in Fig. 4a. Two similar peaks located at around 798 cm^{-1} and 1036 cm^{-1} are observed on the spectra of RHA and CuSi-NTMs. These peaks correspond to the bending vibration of the Si–O bond and the stretching vibration of the Si–O–Si bond, respectively, indicating the presence of silicate tetrahedra. For CuSi-NTMs, the peak at 3615 cm^{-1} is attributed to stretching vibration of Cu–OH, the presence of Cu–OH suggests partial hydrolysis of Cu species during synthesis.[40] The peak at approximately 3453 cm^{-1} is assigned to the –OH stretching vibration of the adsorbed water molecules, confirming the hydrophilic nature of CuSi-NTMs. Hydrophilic surfaces enhance polar reactant adsorption *via* hydrogen bonding, leading to reactant enrichment at the catalyst interface and subsequent acceleration of the reaction.[41] Moreover, the small band centered around 1640 cm^{-1} is the H–O–H bending vibration of adsorbed water, which is consistent with the broad –OH stretching peak at 3453 cm^{-1} and provides further evidence for the hygroscopic nature of the material. The 670 cm^{-1} peak is characteristic of octahedrally coordinated Cu^{2+} in layered silicates, corresponding to the vibrational mode of the Cu–O–Si bond. The 466 cm^{-1} peak reflects Cu–O lattice rigidity, potentially contributing to the enhanced thermal stability of CuSi-NTMs. The surface chemical compositions of CuSi-NTMs were further analyzed by XPS (Fig. 4b). The charging effect on the sample surface was calibrated with reference to the C–C peak at 284.8 eV. As shown in

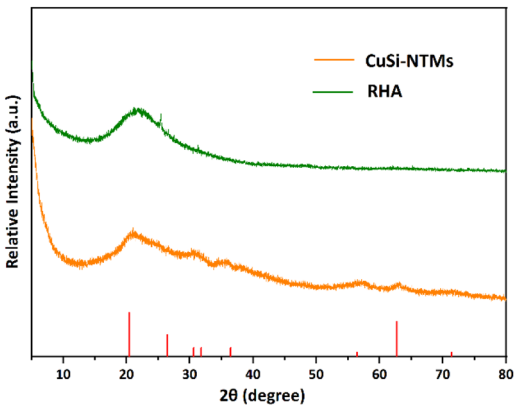

Fig. 3 The XRD patterns of RHA and CuSi-NTMs.

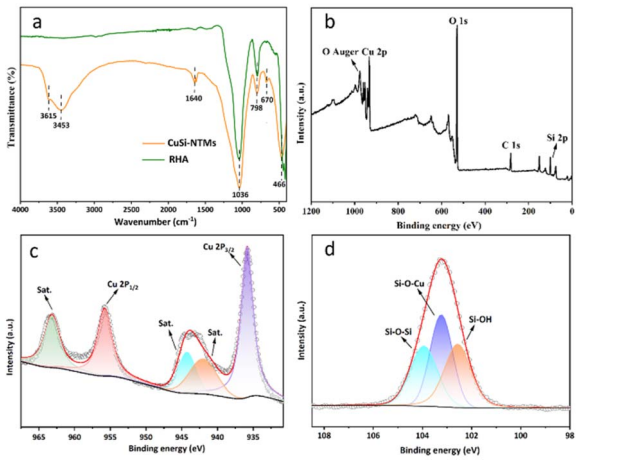

Fig. 4 (a) FTIR spectra of RHA and CuSi-NTMs; (b) full-survey scan XPS spectra of CuSi-NTMs; (c and d) high-resolution XPS spectra of Cu 2p and Si 2p.

Fig. 4c, the high-resolution XPS spectra of Cu 2p suggest that the Cu existed primarily in the form of Cu^{2+}, as evidenced by the binding energies of Cu $2p_{1/2}$ (955.79 eV) and Cu $2p_{3/2}$ (935.83 eV), along with Cu 2p satellite peaks at about 963.17, 944.34 and 942.06 eV. Fig. 4d presents the Si 2p XPS curve of CuSi-NTMs. The two peaks at 103.96 eV (Si–O–Si) and 102.56 eV (Si–OH) confirm the presence of siloxane (Si–O–Si) networks and surface silanol (Si–OH) groups, respectively. Additionally, the peak at 103.23 eV is an indication of the formation of Si–O–Cu bonds, suggesting covalent integration of copper into the silicate framework rather than mere physical adsorption.

The porosity of RHA and CuSi-NTMs was investigated using nitrogen adsorption/desorption isotherms and pore size distribution curves (Fig. 5). The isotherms of the two samples exhibited distinct typical type-IV curves, indicating the presence of mesoporous structures according to IUPAC classification. Pore size distribution curves revealed that mesopores (3–20 nm) were predominant in both samples (inset in Fig. 5). In addition, RHA has a total pore volume (V_{pore}) of 0.261 $cm^3\ g^{-1}$ and a specific surface area (S_{BET}) of 230 $m^2\ g^{-1}$. The CuSi-NTMs shows a significant increase in both V_{pore} and S_{BET}, reaching values of 0.367 $cm^3\ g^{-1}$ and 375 $m^2\ g^{-1}$, respectively. The increase in V_{pore} and S_{BET} of CuSi-NTMs was mainly attributed to the hydrothermal-induced structural reconstruction that generated more mesoporous channels and enhanced the dispersion of active components within the material.

The morphologies of the as-prepared CuSi-NTMs were observed using SEM and TEM analyses. As shown in the SEM image in Fig. 6a, CuSi-NTMs exhibits a spherical morphologies with sizes ranging from 500 nm to 1.5 μm. Fig. 6b provides a magnified view, clearly revealing numerous rod-like protrusions on the surface of the microspheres. The TEM images (Fig. 6c and d) show that CuSi-NTMs exhibit a hollow interior, with microspheres assembled from densely stacked nanotubes. Additionally, a growth mechanism of the CuSi-NTMs hollow microspheres is proposed. After high temperature calcination of RHs and subsequent hydrochloric acid leaching, the RHA exhibits a porous structure. The pore characteristic facilitates preferential nucleation of CuSi-NTMs precursors at pore entrances or surface defects, followed by directional growth along specific crystallographic planes. As the concentration of

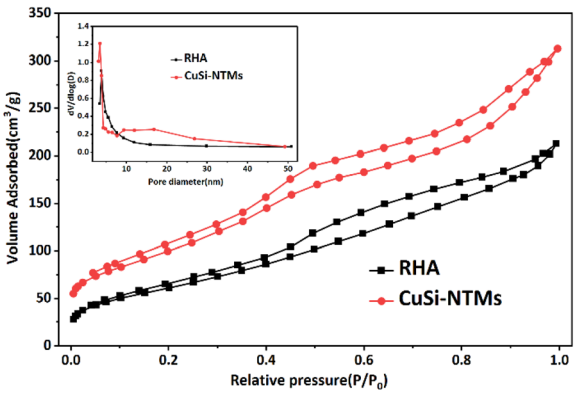

Fig. 5 N_2 adsorption/desorption isotherms of RHA and CuSi-NTMs.

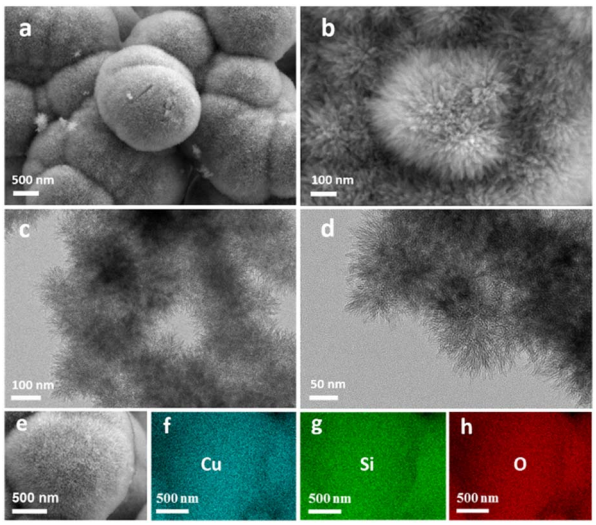

Fig. 6 (a and b) SEM, (c and d) TEM and (e and h) element mapping images of CuSi-NTMs.

SiO_3^{2-} increases, the precursor layer gradually thickens and curls, forming nanotubes. This process is likely driven by surface energy minimization, where nanotubes reduce interfacial energy through curling while maintaining template contact for structural stability. The generated nanotubes grow vertically on the surfaces of RHA. Subsequently, they stack *via* van der Waals forces or hydrogen bonding, forming 3D hollow microspheres. The RHA provides silicon source and templates for the growth of nanotubes, while the coordination of copper-ammonia complex ions regulates the directional deposition of CuSi-NTMs. The synergistic interaction between these two mechanisms enables self-assembly from microscopic coordination to microsphere structures. Such unique morphological feature significantly enhances the adsorption and diffusion efficiency of reactants, expediting the reaction kinetics. Furthermore, the energy-dispersive X-ray spectroscopy (EDS) elemental mapping in Fig. 6e and h reveals that Cu, Si, and O atoms are uniformly distributed on the surface of the CuSi-NTMs microspheres. These results suggest that copper silicate particles have been successfully prepared, consistent with the XRD data.

3.2 Catalysis performance of CuSi-NTMs

We began exploring the initial study with the reaction between 2-methoxy-4-methylphenol **1a** (0.1 mmol) and diethyl azodicarboxylate **2** (0.2 mmol) for condition optimization, with results summarized in Table 1. In the presence of $CuCl_2$ (20 mol%), the dearomatization occurred to afford the corresponding cyclohexadieneone **3a** in 32% yield after 2 h at 25 °C in acetone solvent (Table 1, entry 1). To further refine the catalytic system, we systematically evaluated a series of copper salts (20 mol%), including CuBr, CuI, Cu_2O, $CuSO_4$, $Cu(OAc)_2$ and CuSi-NTMs (entries 2–7). Notably, CuSi-NTMs exhibited the highest product yield, reaching 98%. The possible reason is that the interaction between silicon and the active metal

Table 1 Reaction optimization of dearomatization

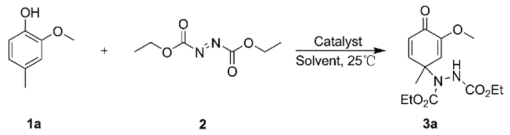

[a]Entry	Catalysts	Solvent	Time (h)	Yield[b] (%)
1	$CuCl_2$	Acetone	2	32
2	CuBr	Acetone	2	35
3	CuI	Acetone	2	58
4	Cu_2O	Acetone	2	63
5	$CuSO_4$	Acetone	2	90
6	$Cu(OAc)_2$	Acetone	2	37
7	CuSi-NTMs	Acetone	2	98
8	CuSi-NTMs	CH_2Cl_2	2	50
9	CuSi-NTMs	Toluene	2	47
10	CuSi-NTMs	THF	2	52
11	CuSi-NTMs	CH_3OH	2	30
12	CuSi-NTMs	DMF	2	34
13	CuSi-NTMs	H_2O	2	64
14	—	Acetone	2	Trace
15	CuSi-NTMs	Acetone	1	70

[a] Reactions were performed with **1a** (0.1 mmol), **2** (0.2 mmol), catalysts (20 mol%) in 1.0 mL of solvent, 25 °C, 2 h. [b] Isolated yield.

components modulates the electronic structure of the catalyst, thereby enhancing its catalytic activity and selectivity. Furthermore, a range of organic solvents were employed to assess the solvent compatibility (entries 8–13). The results revealed that acetone exhibited superior performance among the tested solvents including CH_2Cl_2, toluene, THF, *etc.* In the absence of copper salts, only a trace amount of **3a** was generated, indicating that acetone solvent has no significant influence on the reaction (entry 14). When the reaction time was shortened to 1 h, a decline in yield to 70% was observed (entry 15). Consequently, the conditions shown in entry 7 are selected as the optimized ones.

We systematically investigated the influence of the steric hindrance and electronic effects of phenol derivatives on their dearomatization reactions. Under the optimized conditions, a series of *para*-substituted phenols were subjected to dearomatization with diethyl azodicarboxylate, as shown in Fig. 7. Specifically, substrates bearing alkyl groups with varying degrees of para-steric hindrance (–CH_3, –C_2H_5 and –C_3H_7) were evaluated (**3a–3c**, Fig. S1–S6). Results revealed that dearomatization of phenol derivatives with different steric hindrances gave satisfactory yields (>90%). Notably, the para-methyl-substituted phenol **1a** afforded the desired product **3a** in 98% yield within 2 h under these conditions. To further probe electronic effects, ortho-substituted phenols bearing –CH_3, –F, and –Cl groups were examined (**3d–3f**, Fig. S7–S12). All these substrates reacted smoothly, yielding the corresponding cyclohexadienones in excellent yields, suggesting minimal electronic perturbation from these substituents under the reaction conditions. However, the *ortho*-fluorinated substrate **3e**

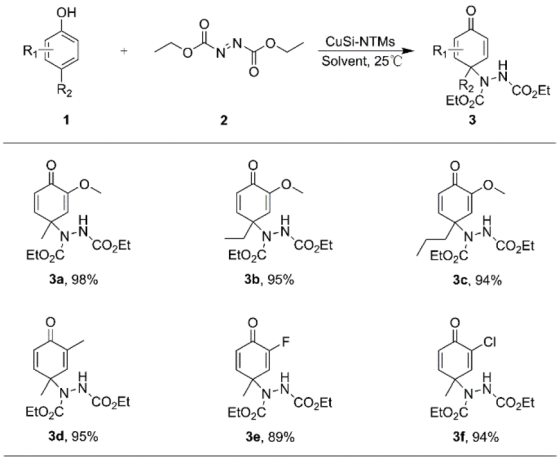

Fig. 7 Substrate scope of dearomatization (0.1 mmol of **1**, 0.2 mmol of **2**, 20 mol% of CuSi-NTMs, 1.0 mL of acetone, 25 °C, 2 h. Isolated yield).

exhibited a slightly lower yield (89%), likely attributable to the stronger electron-withdrawing inductive effect of the fluorine atom compared to the other substituents. In contrast, the *ortho*-methyl-substituted analogue **3d** maintained excellent yield performance (95%), consistent with the electron-donating nature of the methyl group. Additionally, a gram-scale synthesis was conducted using the model substrate. Specifically, compound **1a** (1.38 g, 10 mmol) was reacted with compound **2** (3.48 g, 20 mmol) in 8 mL of acetone at 25 °C for 2 h, giving product **3a** (3.0 g) in 92% yield.

To verify the catalytic mechanism of the CuSi-NTMs, we introduced the radical scavenger TEMPO into the reaction between **1a** and **2**. Control experiments confirmed that the presence of TEMPO did not significantly affect the formation of product **3a** (Fig. S13), which was still obtained in an 88% yield. Notably, this finding eliminates the potential involvement of

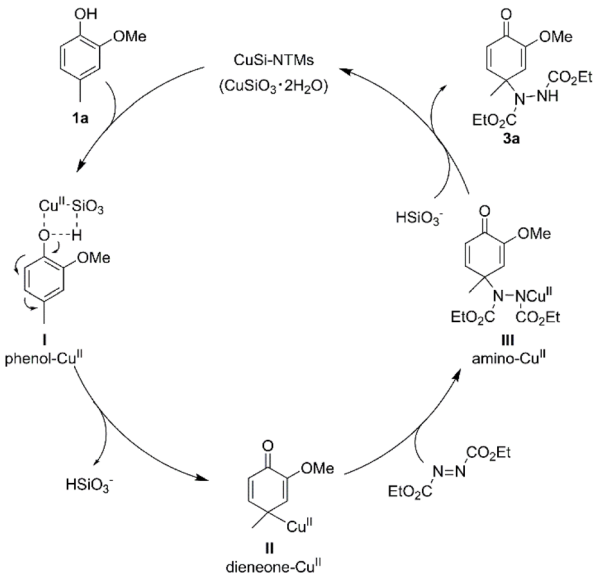

Fig. 8 Plausible mechanism of dearomatization.

a radical-mediated pathway, demonstrating that the reaction proceeds *via* an ionic-catalyzed process. Based on previous study of Cu(II)-catalyzed C–N coupling mechanism,[42] we have proposed a possible mechanism for the dearomatization of phenolic derivatives catalyzed by CuSi-NTMs, as depicted in Fig. 8. In the initial stage of the reaction, the –OH group of 2-methoxy-4-methylphenol **1a** interacts with Cu(II) to form phenol-Cu^{II} complex I. This process activates the para-position of the phenol, thereby facilitating the formation of dieneone-Cu^{II} complex II. Subsequently, complex II undergoes an aza-Michael-type addition reaction with diethyl azodicarboxylate, leading to the generation of the dearomatized amino-Cu^{II} complex III. Finally, the dearomatized product **3a** (cyclohexadienone) is produced through a proton transfer process, while CuSi-NTMs is regenerated to participate in the subsequent catalytic cycle.

4. Conclusions

In summary, we obtained rice husk ash (RHA) with a high silicon content by calcining rice husks (RHs) at 600 °C. By *in situ* utilizing the silicon present in the RHA, we successfully prepared the CuSi-NTMs catalyst. The characterization results of the CuSi-NTMs material reveal its good crystallinity. The material exhibits a hollow microsphere morphology composed of densely stacked nanotubes. Compared with other Cu-based catalysts, the CuSi-NTMs catalyst can efficiently catalyze the dearomatization reaction between phenol derivatives and diethyl azodicarboxylate. Under controlled reaction conditions (25 °C, 2 h, acetone), CuSi-NTMs catalyzed the reaction with a yield reaching 98%, which indicates its superior performance compared to traditional copper-based catalysts. Further studies have shown that the presence of a strong electron-withdrawing group (–F) at the *ortho*-substituted phenols leads to a slight decrease in yield. In addition, the steric effect of para-substituted substituents has minimal impact on the yield, resulting in yields ranging from 89% to 95%. The catalytic mechanism of CuSi-NTMs follows an ionic-catalyzed mechanism. First, the Cu(II) coordinates with the phenolic –OH group, activating its para-position. Then, the activated phenol undergoes a Michael addition reaction with the N=N group, followed by deprotonation, ultimately yielding cyclohexadienone derivatives. Overall, the rational utilization of biomass resources to design catalysts holds great potential to drive the catalytic industry towards green, efficient, and sustainable upgrading.

Author contributions

All authors have equal contribution in writing, formatting, editing, sampling, characterization, analysis.

Conflicts of interest

All authors declare that they have no competing interests.

Data availability

The data supporting this article have been included as part of the supplementary information (SI). Supplementary information: ^{1}H NMR spectrum, ^{13}C NMR spectrum of the product, gas chromatography for the formation mechanism of cyclohexadienone, and further experimental detail. See DOI: https://doi.org/10.1039/d5ra09185c.

Acknowledgements

The authors thank the National Natural Science Foundation of China (32460230), Inner Mongolia Natural Science Foundation (2024QN02016), Talent Research Support Funds from Government-Sponsored Institution of Inner Mongolia of China (RCQD20003), Inner Mongolia Minzu University Doctoral Research Start-up Fund Project (BS623) and Basic Research Funds for University at the Inner Mongolia (GXKY25Z046) for financial support of this work.

References

1 F. Adam, J. N. Appaturi and A. Iqbal, The utilization of rice husk silica as a catalyst: Review and recent progress, *Catal. Today*, 2012, **190**, 2.
2 I. Hamidu, B. Afotey, B. Kwakye-Awuah and D. A. Anang, Synthesis of silica and silicon from rice husk feedstock: A review, *Heliyon*, 2025, **11**, e42491.
3 N. L. Hakkim and L. Nebhani, One-step functionalization and polymer grafting potential of green silica derived from rice husk ash, *Surf. Interfaces*, 2024, **51**, 104505.
4 A. Riyanto, S. Machmudah, S. Y. Purwaningsih and S. Pratapa, Rice husk-based silica: A structural and optical study of xerogel, amorphous, and crystalline phases, *Opt. Mater.*, 2025, **166**, 117115.
5 P. T. Williams and N. Nugranad, Comparison of products from the pyrolysis and catalytic pyrolysis of rice husks, *Energy*, 2000, **25**, 493.
6 R. M. Mohamed, I. A. Mkhalid and M. A. Barakat, Rice husk ash as a renewable source for the production of zeolite NaY and its characterization, *Arab. J. Chem.*, 2015, **8**, 48.
7 Y. Liu, H. Tan, Z. Tan and X. Cheng, Rice husk-derived carbon materials for aqueous Zn-ion hybrid supercapacitors, *Appl. Surf. Sci.*, 2023, **608**, 155215.
8 M. Abbasi, I. Hosseinpour, M. Salimi, A. Ghanbari Astaneh and M. Payan, A comparative study on stabilization efficiency of kaolinite and montmorillonite clays with fly ash (FA) and rice husk ash (RHA)-based geopolymers, *J. Mater. Res. Technol.*, 2025, **36**, 2332.
9 A. Parrillo and G. Sánchez, Coproduction of silicon nitride & oxynitride whiskers and precipitated silica from industrial rice husk ash, *Sustainable. Mater. Technol.*, 2024, **40**, e00871.
10 S. A. Farid and M. M. Zaheer, Production of new generation and sustainable concrete using Rice Husk Ash (RHA): A review, *Mater. Today: Proc.*, 2023, **23**, 1–10.
11 D. D. Andi Grefa, J. E. Guevara Sánchez, L. R. Bravo Sánchez, M. S. Pomares Alfonso and M. E. Villanueva Tagle, Rice husk

ash as sorbent for solid phase extraction of diclofenac, ibuprofen and carboplatin residues from waters, *Microchem. J.*, 2023, **195**, 109361.

12 V. KumarMagotra, A. Magotra, T. W. Kang, S. J. Lee, A. S. mishra, A. Pandey, D. Y. Kim and H. C. Jeon, Fabrication of grey cement brick fuel cell (GC-BFC) using agricultural waste rice husk ash for generating power: A novel approach for smart cities, *Biomass Bioenergy*, 2025, **201**, 108126.

13 S. Zhang, H. Gao, J. Li, Y. Huang, A. Alsaedi, T. Hayat, X. Xu and X. Wang, Rice husks as a sustainable silica source for hierarchical flower-like metal silicate architectures assembled into ultrathin nanosheets for adsorption and catalysis, *J. Hazard. Mater.*, 2017, **321**, 92.

14 H. Moayedi, B. Aghel, M. M. Abdullahi, H. Nguyen and A. S. A. Rashid, Applications of rice husk ash as green and sustainable biomass, *J. Clean. Prod.*, 2019, **237**, 117851.

15 Z. Zhao, S. Feng, Y. Zhao, Z. Wang, J. Ma, L. Xu, J. Yang and B. Shen, Investigation on the fuel quality and hydrophobicity of upgraded rice husk derived from various inert and oxidative torrefaction conditions, *Renew. Energ.*, 2022, **189**, 1234.

16 L. Sun and K. Gong, Silicon-Based Materials from Rice Husks and Their Applications, *Ind. Eng. Chem. Res.*, 2001, **40**, 5861.

17 A. Akshaya, P. Chinnaiyan, D. Unni and G. Keerthana, Use of TiO_2 and Rice Husk Ash to study the removal of Reactive Yellow Dye as contaminant in water, *Mater. Today*, 2018, **5**, 24268.

18 N. Tipsotnaiyana, L. Jarupan and C. Pechyen, Synthesized Silica Powder from Rice Husk for Printing Raw Materials Application, *Adv. Mat. Res.*, 2012, **506**, 218.

19 J. Andas, F. Adam and I. A. Rahman, Sol–gel derived mesoporous cobalt silica catalyst: Synthesis, characterization and its activity in the oxidation of phenol, *Appl. Surf. Sci.*, 2014, **315**, 154.

20 S. Feng, C. Ge, Q. Sun, W. Zheng, G. Li and C. Hu, Valorization of agriculture waste: Preparation of alkoxysilanes from mixed rice straw and rice husk ash, *Chem. Eng. J.*, 2024, **495**, 153377.

21 N. Soltani, A. Bahrami, M. I. Pech-Canul and L. A. Gonzalez, Review on the physicochemical treatments of rice husk for production of advanced materials, *Chem. Eng. J.*, 2014, **264**, 899.

22 J. H. Lee, J. H. Kwon, J.-W. Lee, H.-S. Lee, J. H. Chang and B. I. Sang, Preparation of high purity silica originated from rice husks by chemically removing metallic impurities, *Ind. Eng. Chem.*, 2017, **50**, 79.

23 Y. Zhu, H. Shen, Q. Ai, Y. Feng, B. Shin, M. Gonzales, Y. Yan, Z. He, X. Huang, X. Zhang, Y. Han, P. M. Ajayan, Q. Li and J. Lou, Double Layer SiO_2-Coated Water-Stable Halide Perovskite as a Promising Antimicrobial Photocatalyst under Visible Light, *Nano Lett.*, 2024, **24**, 13718.

24 J. Chen, W. Zhang, D. Huang, J. Wu and X. Wu, Dearomatization of Aromatic Compounds: A Decade Review, *Asian J. Org. Chem.*, 2025, **14**, e00382.

25 M. Li and D.-H. Wang, Copper-Catalyzed 3-Positional Amination of 2-Azulenols with O-Benzoylhydroxylamines, *Org. Lett.*, 2021, **23**, 6638.

26 C. Zheng and S.-L. You, Advances in Catalytic Asymmetric Dearomatization, *ACS Cent. Sci.*, 2021, **7**, 432.

27 J. Cai, J. Yu, X. Cao, L. Huang and B. Yin, Photoredox-Induced Dearomatization of 2-Alkenyl Aromatic Carboxylic Acids with Terminal Alkynes, *ACS Catal.*, 2025, **15**, 9672.

28 Y. Chen, S. K. Jia, X. Xiao, M. C. Wang, L. Huang and G. J. Mei, Catalytic Asymmetric Synthesis of Aza-Quaternary Carbon Cyclohexadieneones Enabled by Aminative Dearomatization of Phenols, *Org. Lett.*, 2023, **25**, 4740.

29 J. C. Ge, Y. Wang, F. W. Guo, X. Kong, F. Hu and S. S. Li, Dearomatization of 3-Aminophenols for Synthesis of Spiro [chromane-3,1'-cyclohexane]-2', 4'-dien-6'-ones via Hydride Transfer Strategy-Enabled [5+1] Annulations, *Molecules*, 2024, **29**, 1012.

30 L. H. Zhu, Y. Z. Cheng and S. L. You, Synthesis of Oxazoline-spirocyclohexadienone via Electrochemical Dearomatization of Phenol Derivatives, *Tetrahedron Lett.*, 2025, **164**, 155622.

31 W. T. Wu, L. Zhang and S. L. You, Catalytic asymmetric dearomatization (CADA) reactions of phenol and aniline derivatives, *Chem. Soc. Rev.*, 2016, **45**, 1570.

32 T. Kato, N. Sahara, S. Akagawa, M. Uyanik and K. Ishihara, Electrochemical oxidative dearomatization of electron-deficient phenols using Br^+/Br^- catalysis, *Chem. Comm.*, 2024, **61**, 2075.

33 Z.-Q. Yang, Y. Gong, Q. Gu and S.-L. You, Rhodium-Catalyzed Asymmetric Allylic Dearomatization of β-Naphthols with gem-Difluorinated Cyclopropanes, *ACS Catal.*, 2025, **15**, 4287.

34 L. Liu, C.-Y. Zhou and C. Wang, Construction of highly congested quaternary carbon centers by NHC catalysis through dearomatization, *Green Synth. Catal.*, 2023, **4**, 263.

35 R. Zhao, Z. Zhou, J. Liu, X. Wang, Q. Zhang and D. Li, Silver-Catalyzed para-Selective Amination and Aminative Dearomatization of Phenols with Azodicarboxylates in Water, *Org. Lett.*, 2020, **22**, 8144.

36 B. Das, S. R. Sahoo, A. Das, B. Pathak and D. Sarkar, Sustainable Organic Photocatalysis for Site-Selective Hydrazocoupling of Electron-Rich Arenes, *Org. Lett.*, 2023, **25**, 7733.

37 F. Adam, J. N. Appaturi and A. Iqbal, The utilization of rice husk silica as a catalyst: Review and recent progress, *Catal. Today*, 2012, **190**, 2.

38 W. Zhao, L. Du, Z. Zhang, F. Guo, Q. Wang, H. Zhang and W. Wang, Controlled epitaxial synthesis of copper silicate nanotube clusters featuring multiple active sites for superior antibiotic removal, *Sep. Purif. Technol.*, 2025, **378**, 134600.

39 X. Wei, C. Tang, X. Wang, L. Zhou, Q. Wei, M. Yan, J. Sheng, P. Hu, B. Wang and L. Mai, Copper Silicate Hydrate Hollow Spheres Constructed by Nanotubes Encapsulated in Reduced Graphene Oxide as Long-Life Lithium-Ion Battery Anode, *ACS Appl. Mater. Interfaces*, 2015, **7**, 26572.

40 Y. Li, K. Nie, Q. Tang, G. Tian and J. Liang, In-situ synthesis of duster-like hollow mesoporous copper silicate composites for high-efficiency adsorption of aflatoxin B1 from water, *Microporous Mesoporous Mater.*, 2022, **346**, 112317.

41 Z. Zeng, S. Shan, R. Peng, Z. Yan and Y. Liu, A hydrophilic porphyrin-based COF to reduce CO_2 and nitrite in situ for photoelectrochemical catalysis for the synthesis of urea, *Chem. Comm.*, 2025, **61**, 8035.

42 T. Ramar, A. Ilangovan, N. A. Meanwell and M. A. M. Subbaiah, Electrophilic Hydrazination of Cyclopropanols Using Azodicarboxylates via Copper(II) Catalysis: An Umpolung Strategy to Access β-Hydrazino Ketone Motifs, *J. Org. Chem.*, 2022, **87**, 14596.